Wefer, G., Berger, W.H., and Richter, C. (Eds.)
Proceedings of the Ocean Drilling Program, Scientific Results Volume 175

9. Data Report: Sedimentation Rates from Milankovitch Periodicity in Log and GRA Bulk Density Records off Southwest Africa, Sites 1081, 1082, and 1084[1]

T.J. Gorgas,[2] J.D. Kronen Jr.,[2] and R.H. Wilkens[3]

ABSTRACT

Sedimentation rates (SR) off the southwest African coast were calculated by performing spectral analyses on borehole and gamma-ray attenuation (GRA) wet bulk density records. Our SR profiles, calculated for selected Sites 1081, 1082, and 1084, Ocean Drilling Program Leg 175, were consistent with those obtained from biostratigraphic analyses in both depth and time domain. However, our calculations revealed greater details in SR variations than those obtained from biostratigraphy because of a much higher sampling rate of GRA bulk density and well-log measurements. We generated high-resolution SR profiles by applying a fast Fourier transform on the autocorrelation function, which was moved over the wet bulk density records. Our method relies on the correct identification of spectral peaks that coincide with Milankovitch cycles. The detection of main orbital periods, namely precession (19 to 23 k.y.), obliquity (41 k.y.), and eccentricity (100 k.y.), allows the conversion of cycles per meter into SR values (meters per million years). Inversion and integration of these SR values yielded high-resolution SR profiles in the time domain.

We calculated a maximal age of ~9.0 Ma for sediments on the Walvis Ridge (Site 1081), and 5.6 and 4.6 Ma in the Walvis Basin (Sites 1082 and 1084, respectively). Sedimentation cycles in the Milankovitch waveband characterized our power spectra at all sites. Waxing and wan-

[1]Gorgas, T.J., Kronen, J.D., and Wilkens, R.H., 2001. Data report: Sedimentation rates from Milankovitch periodicity in log and GRA bulk density records off southwest Africa, Sites 1081, 1082, and 1084. *In* Wefer, G., Berger, W.H., and Richter, C. (Eds.), *Proc. ODP, Sci. Results,* 175, 1–23 [Online]. Available from World Wide Web: <http://www-odp.tamu.edu/publications/175_SR/VOLUME/CHAPTERS/SR175_09.PDF> [Cited YYYY-MM-DD]
[2]Department of Geology and Geophysics, SOEST, University of Hawaii, 1680 East-West Road, Honolulu HI 96822, USA. Correspondence author: **tgorgas@soest.hawaii.edu**
[3]Office of Naval Research Code 322-GG, 800 North Quincy Street, Arlington VA 22217-5660, USA.

Initial receipt: 2 February 2000
Acceptance: 14 September 2000
Web publication: 10 April 2001
Ms 175SR-208

ing of the cycle amplitudes were interpreted as variations in orbital forcing that has influenced heterogeneously local changes in bioproductivity and upwelling vigor across the study area. Time segments of high deposition before 1.2 Ma correlated strongly with a contemporaneous presence of all three Milankovitch cycles, whereas low SR values were noticed when not all of the main cycles coexisted. However, after 1.2 Ma, the correspondence between spectral and deposition patterns was less consistent than before.

We tested our methodology on synthetic density compaction curves that were perturbed with known frequencies. This enabled us to investigate the influence of variable Fourier and autocorrelation windows, smooth factors, noise contamination, and aliasing effects on our results. These models were aimed to optimize our technique in resolving the correct depositional rates at our selected sites by quantifying Milankovitch cyclicity in wet bulk density records.

INTRODUCTION

Orbital climate forcing has long been accepted as one main factor in modifying physical properties of marine sediments and oxygen isotope profiles in a cyclic pattern (Shackleton, 1987; Jansen et al., 1991; Berger, Kroenke, Mayer, et al., 1993; de Boer and Smith, 1994; Cooper, 1995; Kronen and Wilkens, pers. comm., 2000). The study of cyclic variability in marine sediments has enhanced our knowledge of glacio-eustatic and tectonic processes over time (Diester-Haass et al., 1992; Wright and Miller, 1993; Clark et al., 1999; Krijgsman et al., 1999).

We investigated the nature of Milankovitch cyclicity in the form of density variations in hemipelagic sediments off the southwest African coast to obtain a detailed sedimentation rate (SR) history for our study area. We aim to contribute knowledge about the evolution of the Benguela Current upwelling system (BCUS), a coastal upwelling center that is comparable to other large upwelling systems in the world (Berger et al., 1999). We analyzed wireline and gamma-ray attenuation (GRA) bulk density (Boyce, 1976; Gerland and Villanger, 1995), which, in general, provide high-resolution records over long intervals that are quickly obtained and cost effective. For this study we focused on log and GRA bulk density from Ocean Drilling Program (ODP) Sites 1081, 1082, and 1084 (Fig. F1) drilled during Leg 175. The increased sampling rate of log and GRA bulk density at these sites yielded SR histories of greater detail than those obtained from biostratigraphy.

Hemipelagic clays and oozes at Sites 1081, 1082, and 1084 are composed of a varying abundance of diatoms, foraminifers, radiolarians, and nannofossils (Wefer, Berger, Richter, et al., 1998). Our data analyses on these sediment records revealed a cyclic variability in density, which we attributed to orbital forcing in accord with the Milankovitch periods. Variations in density generally observed in geophysical logs are caused by changes in the microstructure of the sediment, which influence physical properties such as porosity, grain size distribution, and type of grain contacts of the sediment (Kronen and Wilkens, pers. comm., 2000). At our study sites the abundance of large foraminifers relative to fine-grained nannofossil ooze (Fig. F2) is linked to bioproductivity and dissolution (Mayer, 1979; Berger and Mayer, 1987; Meyers, 1992) and to diagenetic processes (Wilkens and Handyside, 1985). We suspect that a variable abundance of calcareous foraminifers at these sites (Fig. F2) strongly influences the local variability in density.

F1. Locations of Sites 1081, 1082, and 1084, p. 11.

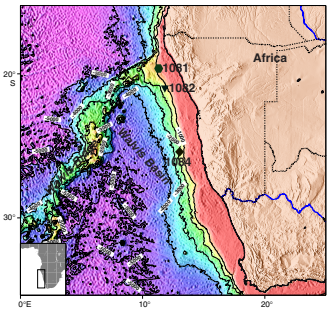

F2. SEM microstructure images, p. 12.

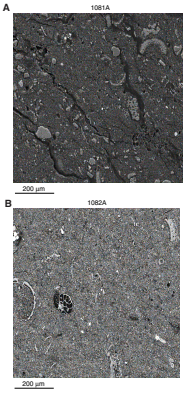

Therefore, we suspect that rhythmic variations in our sediment deposits along the BCUS are linked to the presence of these calcareous microfossils, which maintain intratest porosity to great depths.

METHODS

Log density was acquired during Leg 175 with the Schlumberger lithodensity tool (HLDT) at depth intervals of ~0.15 m (Wefer, Berger, Richter, et al., 1998). GRA bulk density was scanned on board on unsplit cores every 0.02 to 0.04 m to calculate wet bulk density by measuring the amount of gamma-ray attenuation within the formation (Boyce, 1976; Gerland and Villinger, 1995). Density contrasts of as much as 0.8 g/cm³ within thin dolomite horizons at Sites 1081 (Fig. F3A), 1082, and 1084 introduced broadband frequency noise into the power spectra. This noise is similar in character to the Fourier transform of a delta function, showing equal amplitudes throughout the entire frequency spectrum (Smith, 1997). By analyzing cyclic perturbations in synthetic density curves, we found that noise induced by strong density contrasts did not inhibit the correct detection of spectral peaks. A removal of these maximum peaks was disregarded because it would have artificially introduced interruptions in the continuous sediment profile. Subsequent interpolation between all data points and resampling of the entire profile yielded a data point spacing of 0.1524 m for log density (Fig. F3A) and 0.0400 m for the GRA bulk density profiles in the depth domain. A smooth factor, similar to a moving average function, was applied to this resampled density profile (Fig. F3A), which enhanced or reduced certain frequency components. Ideally, the choice of the smooth factor preserved the contemporaneous coexistence of all main orbital periods. We then subtracted the interpolated, smoothed data from the nonsmoothed interpolated profile. We obtained an interpolated residual density record (Fig. F3B), on which we performed our spectral analyses (Fig. F4). Our spectral analysis method consisted of applying a fast Fourier transform (FFT) on the autocorrelation function (Pisias et al., 1973). In this study, we calculated the autocorrelation function over a data window of ~40 m in length (256 points for log density and 1024 points for GRA bulk density records) and applied the FFT (usually 1024 points for log density and 2048 points for GRA bulk density profiles) at the midpoint of this window. Autocorrelation and FFT windows were sufficiently long enough to resolve all main orbital cycles in the frequency domain. The autocorrelation window was passed over the density profile, with a step size of 1.125 m. As a result, each step overlapped the subsequent one to generate a high-resolution profile of evolutionary power spectra over depth.

We extracted SR values (in meters per millions of years) from log and GRA bulk density records by dividing the number of cycles per million years of the individual orbital periods (e.g., obliquity at 41 k.y. occurs ~24 times in 1 m.y.) by their corresponding frequencies (cycles per meter) in our spectra (Fig. F4). We used biostratigraphy as a guide (Berger, Kroenke, Mayer, et al., 1993; Wefer, Berger, Richter, et al., 1998) to provide a working limit or range of SR values, and to facilitate in the identification of orbital parameter frequencies (Kronen and Wilkens, pers. comm., 2000). Calculated SR values were inverted to million years per meter and integrated over depth to generate a high-resolution SR profile as a function of time. We then performed spectral analyses on log and GRA residual bulk density profiles in the time domain to delin-

F3. Log density data, Hole 1081A, p. 13.

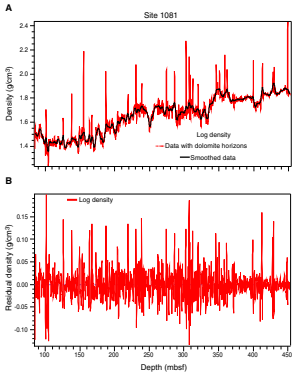

F4. Power spectra of log density in the depth domain, p. 14.

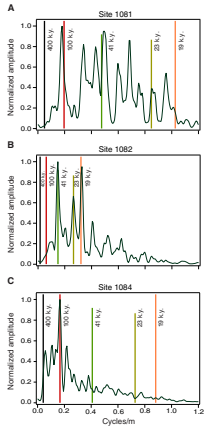

eate the individual orbital cycles. Similar to our data preparation in the depth domain, we resampled the data in the time domain to an equal spacing of 2.0 k.y. The autocorrelation window, which was at least 400 k.y. long to capture both short and long cycles, was passed over the residual density records with a step size of 6 k.y.

For some depth intervals, biostratigraphic SR and calculated values matched very closely so that spectral peaks aligned well with most of the Milankovitch periods (Fig. F4A, F4B). In cases when spectral peaks matched only with one of the Milankovitch cycles in the depth domain (Fig. F4C), we checked whether a different smooth function would enhance other frequencies, or whether only one frequency component was dominant. If a change in the smooth factor did not alter our result, autocorrelation windows were expanded in the depth and time domain to capture more cycles per meter and cycles per million years. In a last step, SR values were fine-tuned in the depth domain, which in return improved the alignment of power spectra with Milankovitch cycles in the time domain. This iterative process optimized the detection of excursions in calculated SR values that often differed from rates established through biostratigraphy. We wanted to ensure the validity of our technique, by applying spectral analyses on synthetic density compaction curves that were perturbed with known frequencies. These model studies provided an opportunity to test how the accuracy of our results was affected by variation of the individual analysis parameters, and will be discussed below.

RESULTS

Sedimentation Rates vs. Depth

Calculated high-resolution SR values in the depth domain overall exhibited a strong correlation with those obtained by biostratigraphy (Fig. F5). Similar to biostratigraphic profiles, our SR values sometimes changed abruptly, but additionally showed much higher resolution excursions. The most pronounced drop in SR values occurred at Site 1084 (Fig. F5C) at ~200 mbsf, from ~315 to 180 m/m.y. Rates at Site 1082 (Fig. F5B) declined more gradually than at Site 1084, from 290 to 120 m/m.y. between 220 and 260 mbsf. In contrast, SR values at Site 1081 (Fig. F5A) on the Walvis Ridge were generally lower compared to Sites 1082 and 1084 in the Walvis Basin and varied only between 35 and 60 m/m.y. below 200 mbsf. However, a strong correlation in high SR peaks was found within the top 150 mbsf between all three sites. Below 200 mbsf, this correlation was not so strong, with the most pronounced SR variations found at Site 1084 between 300 and 600 mbsf (Fig. F5C).

Sedimentation Rates vs. Age

Calculated SR values in the time domain generally followed the trend of the biostratigraphic profiles (Fig. F6). Age-depth relations (A_A to C_C, inset in Fig. F6), derived from our spectral analyses, yielded maximum ages of ~9.0 Ma at Site 1081 (Fig. F6A), 5.3 Ma at Site 1082 (Fig. F6B), and 4.9 Ma at Site 1084 (Fig. F6C). The largest discrepancy in the age-depth profiles was found at Site 1082 between 2.2 and 5.3 Ma (inset B_B in Fig. F6).

A strong correlation in SR values for GRA bulk density was observed at Sites 1081 and 1082 between 0.2 and 0.5 Ma (Fig. F6A, F6B). In con-

F5. Sedimentation rates vs. depth for Sites 1081, 1082, and 1084, p. 16.

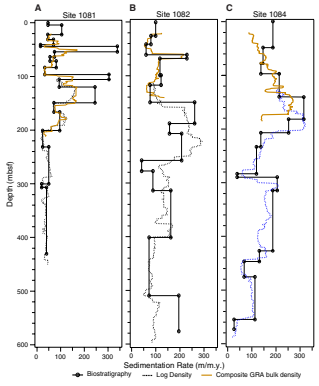

F6. Sedimentation rates vs. age at Sites 1081, 1082, and 1084, p. 17.

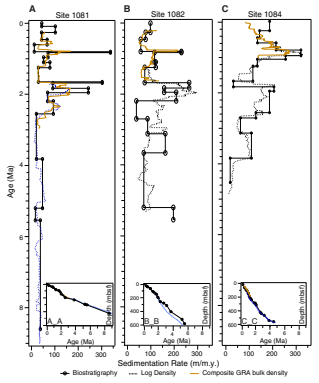

trast, computed data at Site 1084 showed a negative correlation for this time period with the other sites (Fig. F6C). Very pronounced pulses of high deposition rates (150 m/m.y. and greater) were found at all three sites between ~0.7 and 1.05 Ma. The highest variability in SR values (100 to 290 m/m.y.) and the broadest peak (~290 m/m.y.) was observed at Site 1084 (Fig. F6C). A rapid decline in deposition at all sites was found roughly between 1.1 and 1.7 Ma. A rapid increase in deposition around 1.7 Ma and pulses of high SR values until 2.6 Ma characterized deposition at all three sites, with the broadest peak identified at Site 1084 (Fig. F6C).

Before 2.7 Ma, a strong correlation between maximal and minimal SR values among the three sites could not be clearly defined. At Site 1082 (Fig. F6B), a pulse of high SR was found between 2.9 and 3.1 Ma, whereas at Site 1084 (Fig. F6C) an interval of high SR values existed between 3.1 and 3.8 Ma. Log density data obtained at Site 1081 did not correspond to this trend (Fig. F6A). In contrast, Site 1081 revealed relatively high SR values between 4.1 and 5.0 Ma, which was paralleled by a short burst of high deposition rate at Site 1082 only between 4.6 and 4.8 Ma (Fig. F6B). Data obtained at Site 1084 (Fig. F6C) suggested the opposite trend, with low SR values within this particular time period.

Power Spectra in the Time Domain

Evolutionary power spectra as a function of age were generated by applying our spectral analysis technique on residual GRA bulk and log density records in the time domain. Our results showed a strong presence of Milankovitch periodicity (Figs. F7, F8). During some intervals, all three Milankovitch cycles appeared contemporaneously in the spectral waveband, whereas other time periods were predominated only by one or two of the main cycles. Thus, the key observation in our spectral profiles was the waxing and waning of various cycles over time, shifting either abruptly or gradually from one frequency into another.

Strong eccentricity was recognized for the past 1.5 m.y., whereas frequencies in the obliquity and precession waveband appeared to be less pronounced (Fig. F7). Around 1.6 Ma, the dominance of eccentricity waned (Figs. F7A, F8C) and amplitudes of the obliquity cycles became more amplified. All three cycles coexisted in the waveband between 2.0 and 2.6 Ma, whereas before 2.6 Ma mainly eccentricity governed the spectral energy. Practically no obliquity and precession were observed between 3.5 and 4.0 Ma, with slight variations in their times of occurrence among the individual sites (Fig. F8). All three cycles showed strong spectral amplitudes at Site 1081 between 4.2 and 4.8 Ma (Fig. F8A). Before 4.8 Ma, spectral energy records at Site 1081 suggested a pronounced wax-and-wane pattern only between eccentricity and obliquity, but not a strong presence of precessional cycles.

DISCUSSION

Intervals of high SR values along the southwest African coast correlated with intervals of high bioproductivity for the past 1.2 m.y. (Lin et al., 1999). We attributed this and other periods of high SR values to vigorous coastal upwelling in concert with glaciation periods in the Northern and Southern Hemispheres (Keigwin, 1987; Meyers, 1992; Barker, Camerlenghi, Acton., et al., 1999).

F7. Spectral power in the time domain, Sites 1081, 1082, and 1084, p. 18.

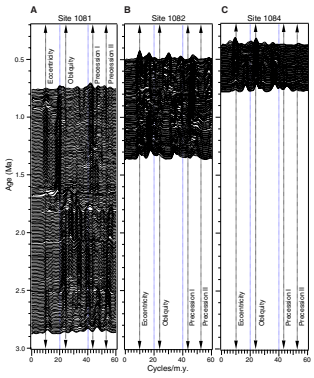

F8. Spectral energy detected in log density profiles over time, Sites 1081, 1082, and 1084, p. 19.

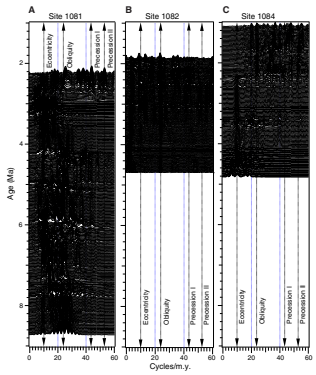

Modeling

We tested our methodology by designing synthetic density curves using a spectral analysis of both the depth and time domains. These artificial density curves represent an accumulative summation over time of a three-component sediment composite (calcareous, siliceous, and clay), which experiences compaction. We tested different SR scenarios over depth, including a constant accumulation rate (Fig. F9A, F9D), a very rapid increase in accumulation (Fig. F9B, F9E), and a smooth increase in rates (Fig. F9C, F9F). Experimental studies on various deep-sea marine sediments provided regression equations for our synthetic compaction curves (Hamilton, 1976). Moreover, we perturbed our synthetic density curves in the depth domain with five sinusoidal cycles, equivalent to 100, 41, 23, 19, and 10 k.y. (Fig. F9). One goal of our modeling was to reproduce these five frequencies in the time domain, utilizing spectral analysis.

At first, we kept accumulation rates of all three components constant (Fig. F9A, F9D) and varied only the smooth factor, but not the autocorrelation and FFT window length (Fig. F10A). High smooth factors resulted in a better detection of low frequencies. Consequently, we attempted to choose a smooth factor for the real wet bulk density data, which prevented the suppression of one Milankovitch component over the others. Next, we only changed autocorrelation window lengths, which showed that lower frequencies were enhanced by longer windows (Fig. F10B). In contrast, higher frequencies were not resolved as clearly as with shorter windows. In addition, they were significantly smeared and displaced over a certain frequency band, erroneously suggesting cycles that were not part of the original waveband. This distortion of the original input frequencies could possibly explain spectral signals in our geologic records that deviated from the expected Milankovitch periodicity (Figs. F7, F8). We point out that this smearing of frequencies reflected a numerical effect, not one from orbital forcing. Frequencies were even more distorted when we introduced broadband frequency noise by incorporating strong high-density contrasts into the synthetic residual density curve (Fig. F10C).

A major goal of our modeling was to quantify the accuracy of our analysis technique. Therefore, we tested the behavior of evolutionary spectra in the depth (Fig. F11) and time domain (Fig. F12) for constant and varying accumulation rates (Fig. F9). Moreover, these model studies shed light on possible aliasing effects caused by undersampling of either synthetic or real-data records. Evolutionary spectra in the depth domain exhibited a gradual increase in spectral frequencies for constant accumulation rate values (Fig. F11A). This reflected an apparent increase in cycles per meter (cycles/m) caused by compaction. A doubling in accumulation of the calcareous component over a short depth interval caused significant deflections of the spectra (Fig. F11B). The deflections were smoother in the case of a gradual accumulation rate increase (Fig. F11C). This test provided means to identify significant and subtle changes in SR values over depth in our geologic records (Fig. F5).

Compaction, which apparently increased frequencies in the depth domain (Fig. F11A), was eliminated in the age domain for constant and varying SR values as long as their original input rates were reproduced correctly. In the case of constant deposition, evolutionary spectra in the age domain exhibited an almost constant frequency value (measured in cycles per million years) over the entire time range (Fig. F12A). However, the 10-k.y. cycle showed a relatively strong deflection from a

F9. Synthetic sedimentation rates of sediment composites, p. 20.

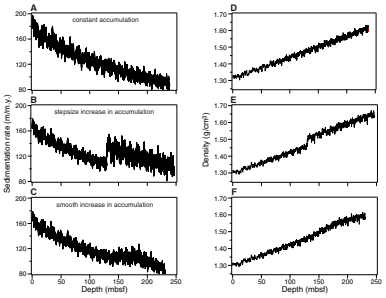

F10. Parameters that influenced results from spectral analyses, p. 21.

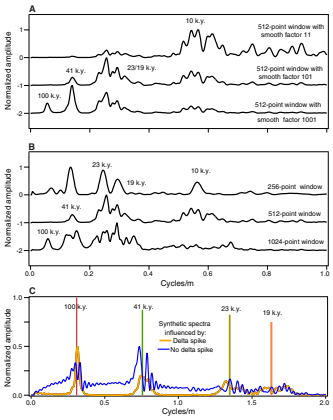

F11. Evolutionary spectra with depth, p. 22.

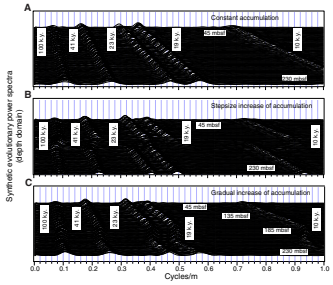

F12. Evolutionary spectra from synthetic density profiles, p. 23.

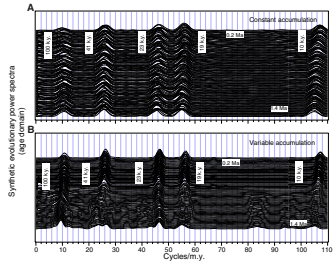

straight spectral path (Fig. F12A), which we attributed to aliasing effects. In general, the difference between input and output frequencies for constant SR values ranged within an acceptable 1%–3%.

In contrast, drastic changes in SR values caused significant deflections in some of the evolutionary spectra from their expected path (Fig. F12B). Consequently, ages obtained from inversion and integration of calculated SR values were off by 10% and more, depending on the frequency component. A drastic shift in SR values affected the individual frequency components not only differently, but also inconsistently (Fig. F12B). Eccentricity (100 k.y.) and the 23-k.y. precessional cycle were deflected less than obliquity (41 k.y.) and the 19-k.y. precessional cycle, whereas the 10-k.y. cycle almost disappeared when accumulation rates changed from low to high values. Below this transition interval, most of the 10-k.y. spectral energy was folded into the lower frequency range because of the strong aliasing, superimposing the other input frequencies (Fig. F12B). We interpreted the observed spectral deflections as the combined effect of aliasing of the various cycles, and of variable autocorrelation window lengths and smooth factors. Therefore, results from our model studies served as an important guide on how to interpret deflections of spectra in the depth domain in order to calculate SR values correctly. Modeling, thus, also improved the delineation of the individual cycles in the age domain.

SUMMARY

GRA bulk and log density data obtained at Sites 1081, 1082, and 1084 allowed the calculation of high-resolution SR in the depth and time domain. Our profiles generally agreed with those from biostratigraphic analyses. We believe that the upwelling history of the BCUS can be explained in part by orbital forcing by influencing indirectly the complex ocean and atmospheric circulation patterns along the southwest African coast over time (Diester-Haass et al., 1992). Accordingly, upwelling vigor varied spatially and temporally, causing a heterogeneous distribution of bioproductivity. This controlled the variability of the SR history along the BCUS, which was further modified by coastal runoff during glacial and interglacial periods (Meyers, 1992).

Results from modeling cyclic variations in simplified synthetic density compaction curves reminded us that caution is required when interpreting periodicity in real geologic records. Our analyses of wet bulk density from log and GRA bulk density records obtained at Sites 1081, 1082, and 1084 (Figs. F7, F8) certainly exhibited some of the phenomena demonstrated with our synthetic density models (Figs. F9, F10, F11, F12). Our theoretical results corresponded with similar studies (Herbert, 1994), suggesting that rapid fluctuations in accumulation rates along the southwest African coast may have caused irregularities in evolutionary power spectra. These, in return, must have affected the accuracy of our method to deduce a high-resolution SR history from spectral analyses. Synthetic accumulation rate profiles, perturbed by a known cyclicity, revealed irregular deviations in power spectra as the result of aliasing (not enough cycles were resolved at a given sampling rate), effects of certain autocorrelation and FFT window lengths, and the choice of smooth factors. The presence of very strong density gradients in our geologic records (delta spikes) introduced broadband noise into the spectral profiles and thus complicated a clear separation of the individual cycles.

In summary, we feel comfortable about our interpretation of wet bulk density data obtained at Sites 1081, 1082, and 1084 because of a reasonable agreement with biostratigraphic analyses (Figs. F5, F6). Conclusions about the upwelling history of the BCUS drawn from previous studies (e.g., Diester-Haass et al., 1999) and about cyclicity from this and other locations (e.g., Meyers, 1992; Clark et al., 1999) confirm the reliability of our results.

ACKNOWLEDGMENTS

We thank the captain and the crew of the *JOIDES Resolution*, both co-chief scientists, W.H. Berger and G. Wefer, ODP Staff Scientist C. Richter, and the entire Shipboard Scientific Party of Leg 175 for their great assistance at sea. This research was supported by a postcruise *JOI/USSSP* grant. Helpful suggestions were made by Dr. Mike Garcia, Denise J. Hills, Stephen J. Leslie, and Tara M. Hicks. Reviews by Lona Dearmont and Jens Grützner greatly enhanced both editorial style and scientific content.

REFERENCES

Barker, P.F., Camerlenghi, A., Acton, G.D., et al., 1999. *Proc. ODP, Init. Repts.,* 178 [Online]. Available from World Wide Web: <http://www-odp.tamu.edu/publications/178_IR/178TOC.HTM>. [Cited 2000-02-02]

Berger, W.H., Kroenke, L.W., Mayer, L.A., et al., 1993. *Proc. ODP, Sci. Results,* 130: College Station, TX (Ocean Drilling Program).

Berger, W.H., and Mayer, L.A., 1987. Cenozoic paleoceanography 1986: an introduction. *Paleoceanography,* 2:613–624.

Berger, W.H., Wefer, G., Richter, C., 1999. Benguela current and Angola-Benguela upwelling systems: preliminary results from Leg 175. *JOIDES J.,* 24:7–9.

Boyce, R.E., 1976. Definitions and laboratory techniques of compressional sound velocity parameters and wet-water content, wet-bulk density, and porosity parameters by gravimetric and gamma-ray attenuation techniques. *In* Schlanger, S.O., Jackson, E.D., et al., *Init. Repts. DSDP,* 33: Washington (U.S. Govt. Printing Office), 931–958.

Clark, P.U., Alley, R.B., and Pollard, D., 1999. Northern hemisphere ice-sheet influences on global climate change. *Science,* 286:1104–1111.

Cooper, P., 1995. Milankovitch cycles from Fourier analysis of logs from Site 865 and 866. *In* Winterer, E.L., Sager, W.W., Firth, J.V., and Sinton, J.M. (Eds.), *Proc. ODP, Sci. Results,* 143: College Station, TX (Ocean Drilling Program), 317–327.

de Boer, P.L., and Smith, D.G., 1994. Orbital forcing and cyclic sequences. *Spec. Publ. Int. Assoc. Sedimentol.,* 19:1–14.

Diester-Haass, L., Bickert, T., Vidal, L., and Wefer, G., 1999. Late Miocene changes in paleoproductivity an carbonate dissolution in the Benguela Current upwelling system: local or global control? *Eos,* 80:F588.

Diester-Haass, L., Meyers, P.A., and Rothe, P., 1992. The Benguela Current and associated upwelling on the southwest African margin: a synthesis of the Neogene-Quaternary sedimentary record at DSDP Sites 362 and 352. *In* Summerhayes, C.P., Prell, W.L., and Emeis, K.C. (Eds.), *Upwelling Systems: Evolution Since the Early Miocene.* Geol. Soc. Spec. Publ. London, 64:331–342.

Gerland, S., and Villinger, H., 1995. Nondestructive density determination on marine sediment cores from gamma-ray attenuation measurements. *Geo-Mar. Lett.,* 15:111–118.

Hamilton, E.L., 1976. Variations of density and porosity with depth in deep-sea sediments. *J. Sediment. Petrol.,* 46:280–300.

Herbert, T.D., 1994. Reading orbital signals distorted by sedimentation: models and examples. *In* de Boer, P.L., and Smith, D.G. (Eds.), *Orbital Forcing and Cyclic Sequences.* Spec. Publ. Int. Assoc. Sedimentol., 19:483–507.

Jansen, E., Mayer, L., and Shipboard Scientific Party, 1991. GRAPE density records and density cyclicity. *In* Kroenke, L.W., Berger, W.H., Janecek, T.R., et al., *Proc. ODP, Init. Repts.,* 130: College Station, TX (Ocean Drilling Program), 553–556.

Keigwin, L.D., 1987. Pliocene stable-isotope record of Deep Sea Drilling Project Site 606: sequential events of ^{18}O enrichment beginning at 3.1 Ma. *In* Ruddiman, W.F., Kidd, R.B., Thomas, E., et al., *Init. Repts. DSDP,* 94 (Pt. 2): Washington (U.S. Govt. Printing Office), 911–920.

Krijgsman, W., Hilgen, F.J., Raffi, I., and Sierro, F.J., 1999. Chronology, causes and progression of the Messinian salinity crisis. *Nature,* 400:652–655.

Lin, H.-L., Lin, C.-Y., and Meyers, P.A., 1999. Late Quaternary changes in marine productivity along the Southwest Africa margin. *Eos,* 80:F568.

Mayer, L.A., 1979. Deep sea carbonates: acoustic, physical, and stratigraphic properties. *J. of Sediment. Petrol.,* 49:819–836.

Meyers, P.A., 1992. Organic matter variations in sediments from DSDP sites 362 and 532: evidence of upwelling changes in the Benguela Current upwelling system. *In*

Summerhayes, C.P., Prell, W.L., and Emeis, K.C. (Eds.), *Upwelling Systems: Evolution Since the Early Miocene*. Geol. Soc. Spec. Publ. London, 64:323–329.

Pisias, N.G., Dauphin, J.P., and Sancetta, C., 1973. Spectral analysis of late Pleistocene-Holocene sediments. *Quat. Res.,* 3:3–9.

Shackleton, N.J., 1987. Oxygen isotopes, ice volume, and sea level. *Quat. Sci. Rev.,* 6:183–190.

Smith, S.W., 1997. *The Scientist's Guide to Digital Signal Processing:* San Diego, California (California Technical Publishing).

Wefer, G., Berger, W.H., and Richter, C., et al., 1998. *Proc. ODP, Init. Repts.,* 175: College Station, TX (Ocean Drilling Program).

Wilkens, R.H., and Handyside, T., 1985. Physical properties of equatorial Pacific sediments. *In* Mayer, L., Theyer, F., Thomas, E., et al., *Init. Repts. DSDP,* 85: Washington (U.S. Govt. Printing Office), 839–847.

Wright, J.D., and Miller, K.G., 1993. Southern Ocean influences on Late Eocene to Miocene deep-water circulation. *In* Kennett, J.P., and Warnke, D.A. (Eds.), *The Antarctic Paleoenvironment: A Perspective on Global Change.* Antarct. Res. Ser., 60:1–25.

Figure F1. Locations of Sites 1081, 1082, and 1084 off southwest Africa. Bathymetry is in meters below sea level.

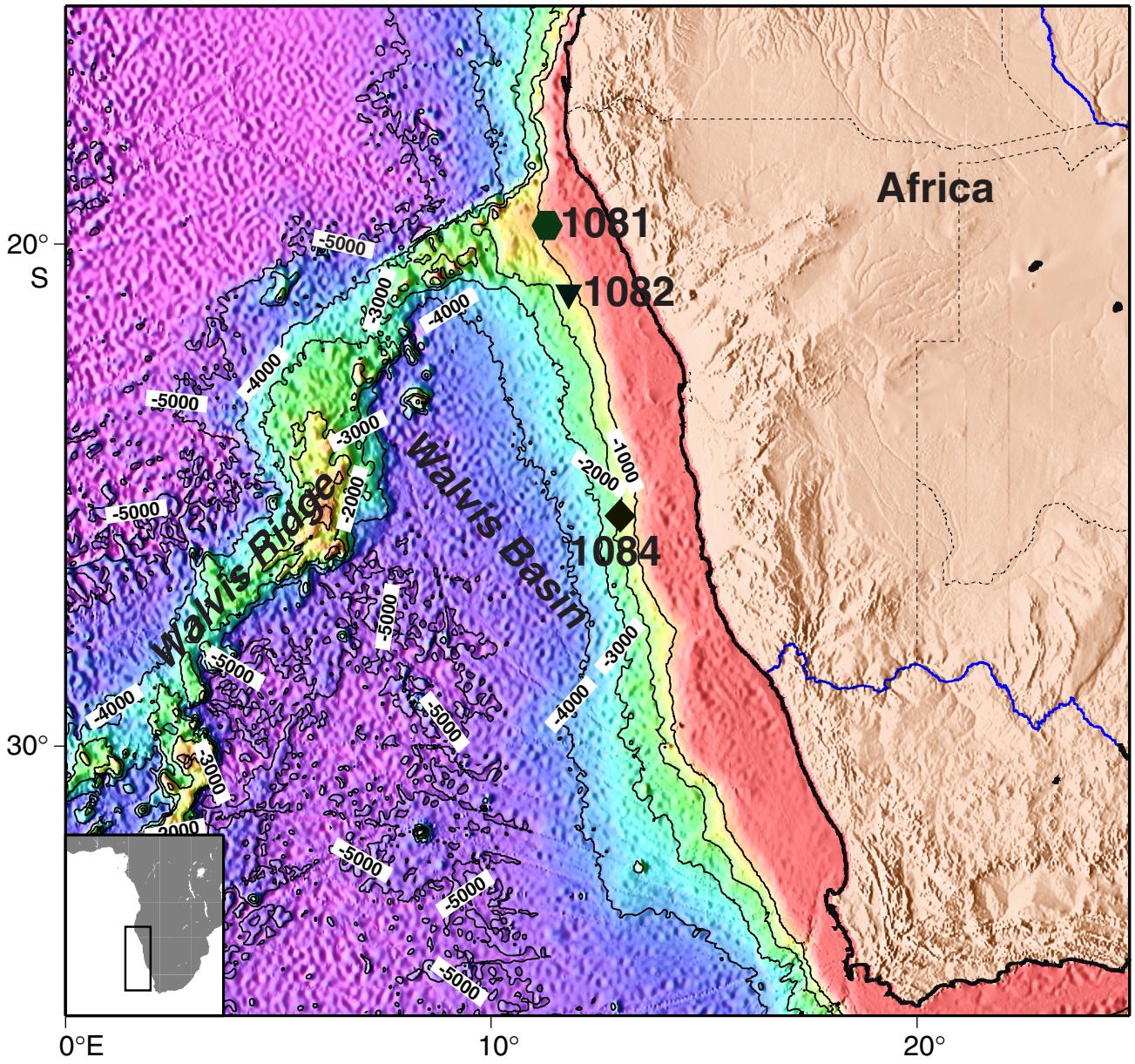

Figure F2. SEM microstructure images. **A.** Hole 1081A at 320 mbsf and 5.8 Ma. A fine-grained clay matrix and a low abundance of calcareous material resulted in darker color and lower reflectance values. **B.** Hole 1082A at 596 mbsf and 5.6 Ma. A fine-grained matrix of calcareous ooze caused lighter color and higher reflectance values. Note the large foraminifers (calcareous microfossils), which retain intratest porosity to great depths.

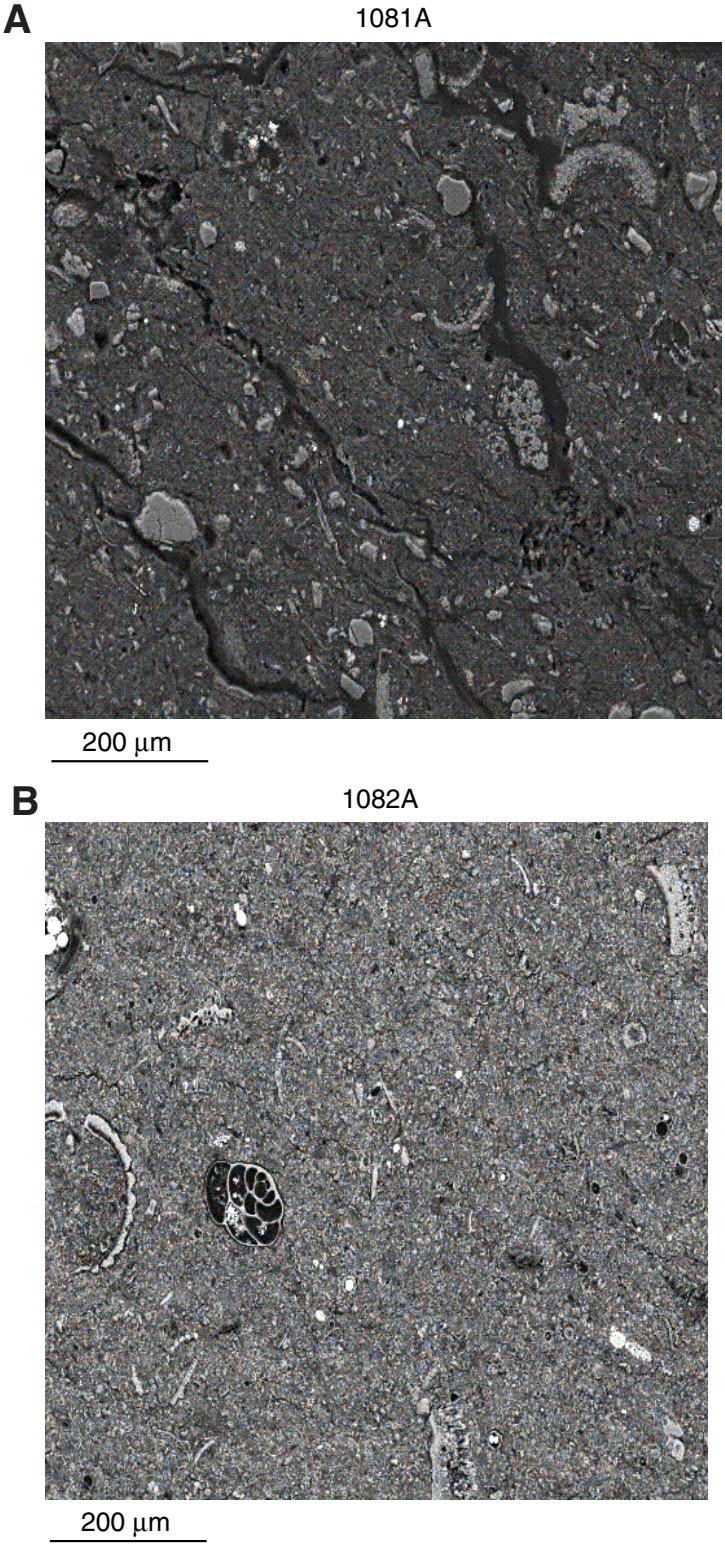

Figure F3. Log density data at Hole 1081A. (**A**) Original data contain strong density contrasts due to the presence of dolomite horizons (stippled line). Data in (A) are interpolated (solid gray line) and smoothed (black line). Subtraction of the smoothed data profile from the interpolated data yields (**B**) an interpolated residual density profile on which spectral analyses were performed.

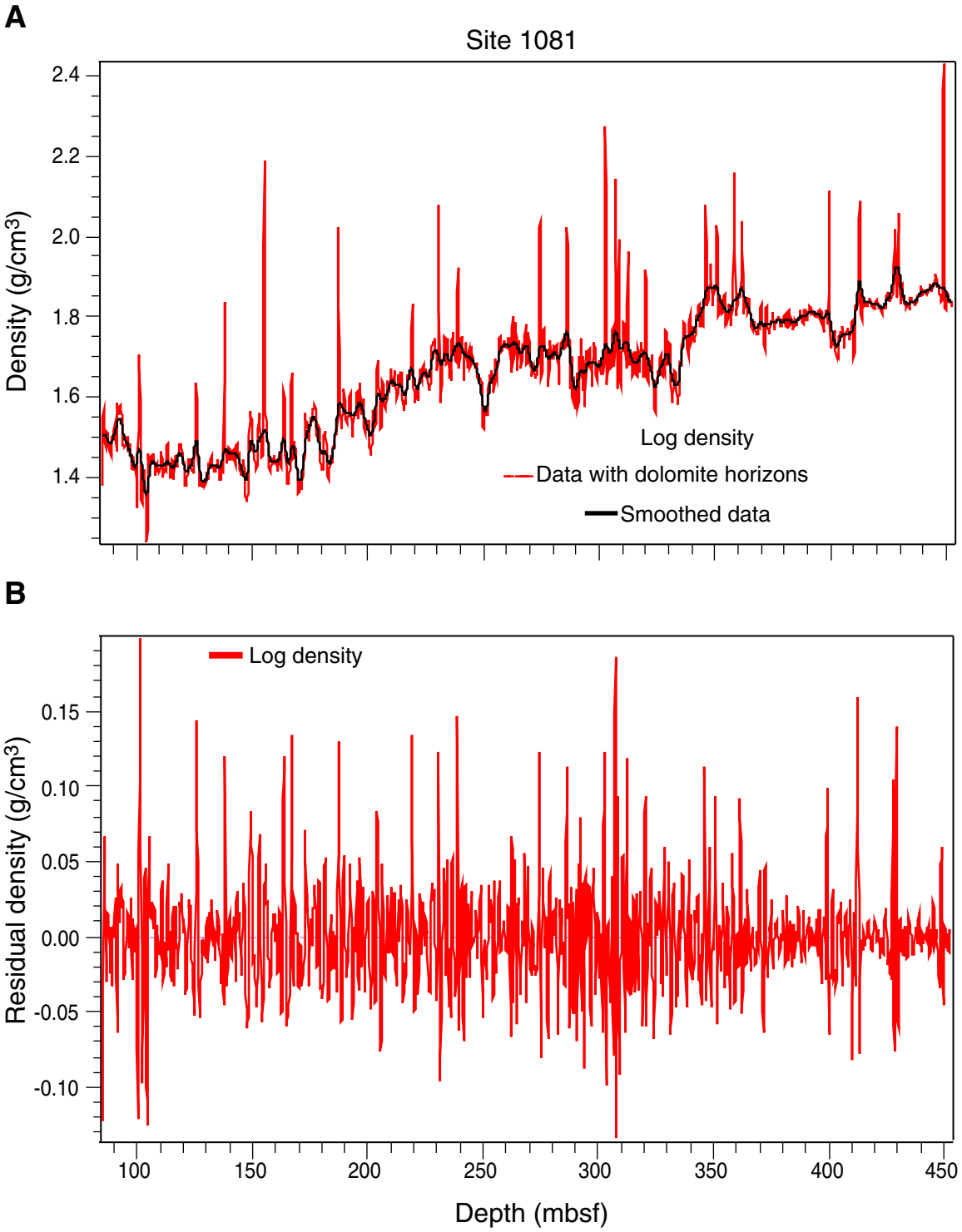

Figure F4. Power spectra of log density in the depth domain. **A.** Site 1081, 259 mbsf, with a calculated sedimentation rate of 51 m/m.y. and an age of ~4.4 Ma. The autocorrelation window (ACW) length is 512 points, and a fast Fourier transform (FFT) window length is 1024 points. **B.** Site 1082, 375 mbsf, with a calculated SR value of 164 m/m.y. and an age of ~3.1 Ma, using the same ACW and FFT lengths. **C.** Site 1084, 467 mbsf, with a calculated SR of 59 m/m.y. and an age of ~3.0 Ma, using the same ACW and FFT lengths. Note the different alignment of spectral peaks with the main orbital periods, induced by ACW and FFT window lengths, smooth factors, and problems with aliasing. (**Figure shown on next page.**)

Figure F4 (continued).

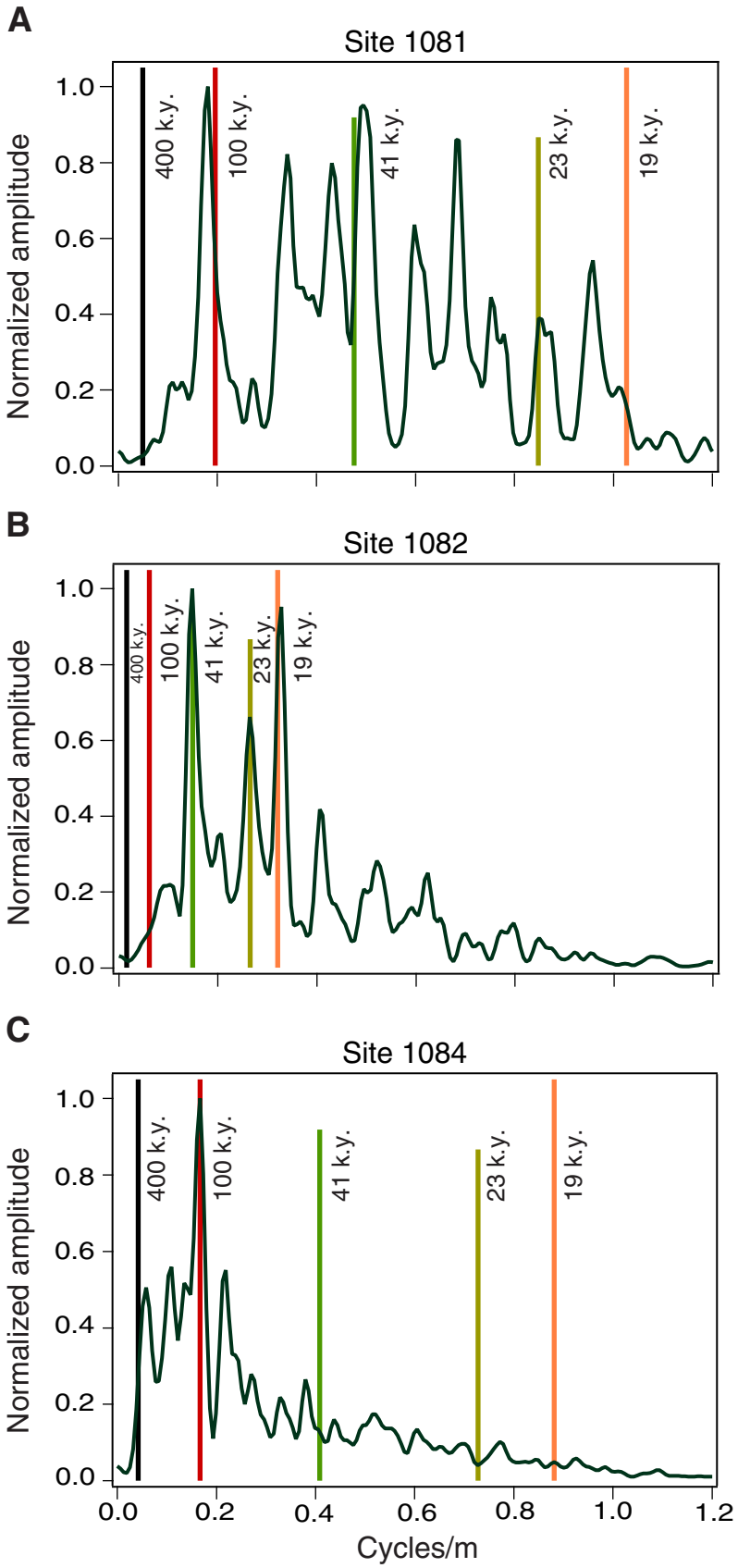

Figure F5. Sedimentation rates (SR) vs. depth for Sites (A) 1081, (B) 1082, and (C) 1084, which correspond well to those from biostratigraphy. The maximum values are from the Walvis Basin at Site 1084 between 100 and 200 mbsf. Differences between SR values suggested by biostratigraphy and our calculated rates are attributed to the significant difference in resolution between log and GRA bulk density records compared to biostratigraphic profiles.

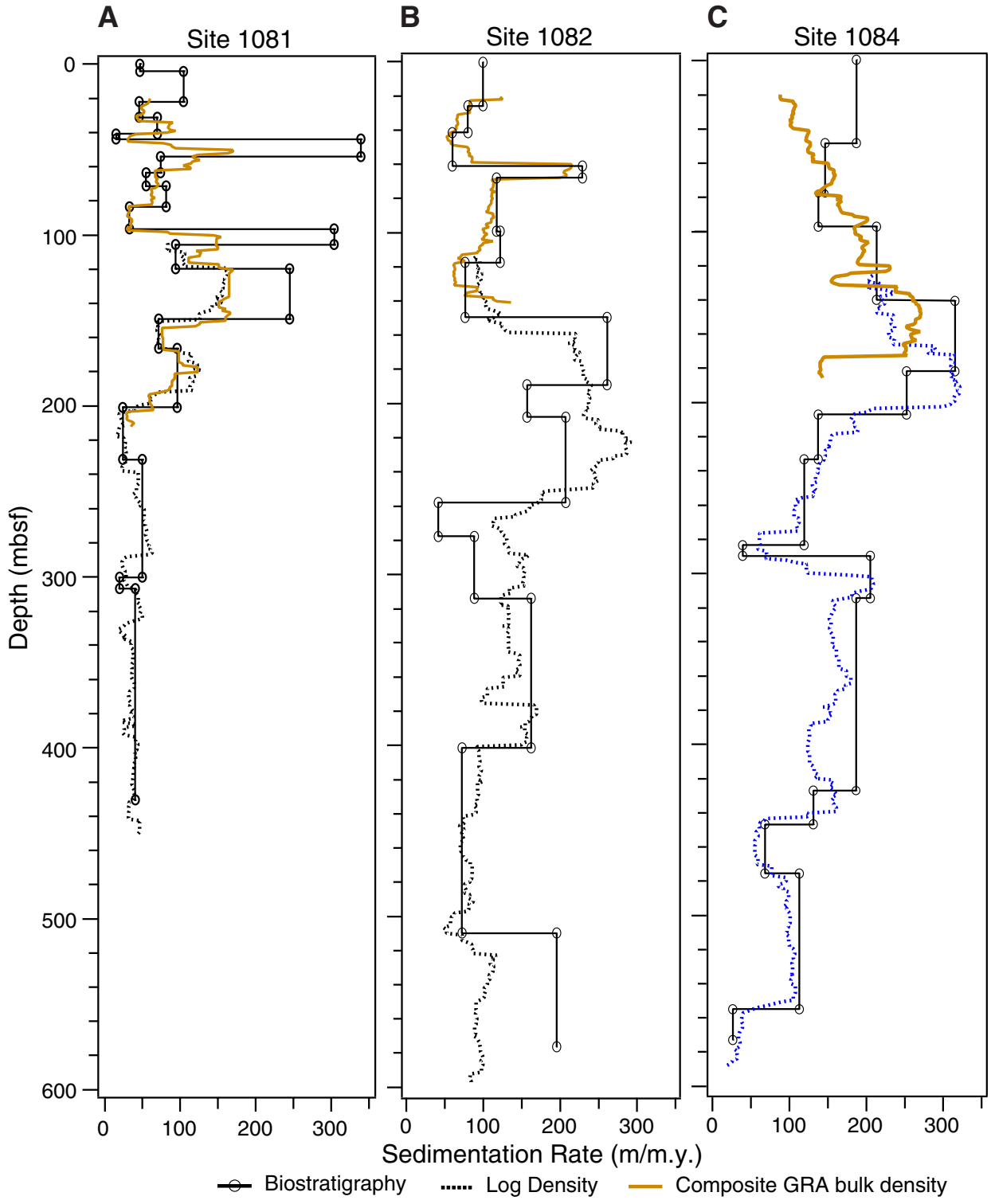

Figure F6. Sedimentation rates (SR) vs. age. **A.** Site 1081 shows maximal peaks between 0.8 and 1.0 Ma and between 1.85 and 2.2 Ma. **B.** Site 1082 exhibits similar trends for the same time period but additionally reveals high SR values between 3.2 and 3.8 Ma and at ~5.2 Ma. **C.** At Site 1084 maxima occur between 0.7 Ma and 1.0 Ma and between 2.0 and 2.8 Ma. A correspondence in values between Sites 1084 and 1082 is observed between 3.2 and 3.8 Ma. Age-depth plots for (A_A) Site 1081, (B_B) Site 1082, and (C_C) Site 1084, inserted into their corresponding SR-age plots, show good agreement between biostratigraphy and GRA bulk and log density data, except at Site 1082 before 2.4 Ma (see inset B_B).

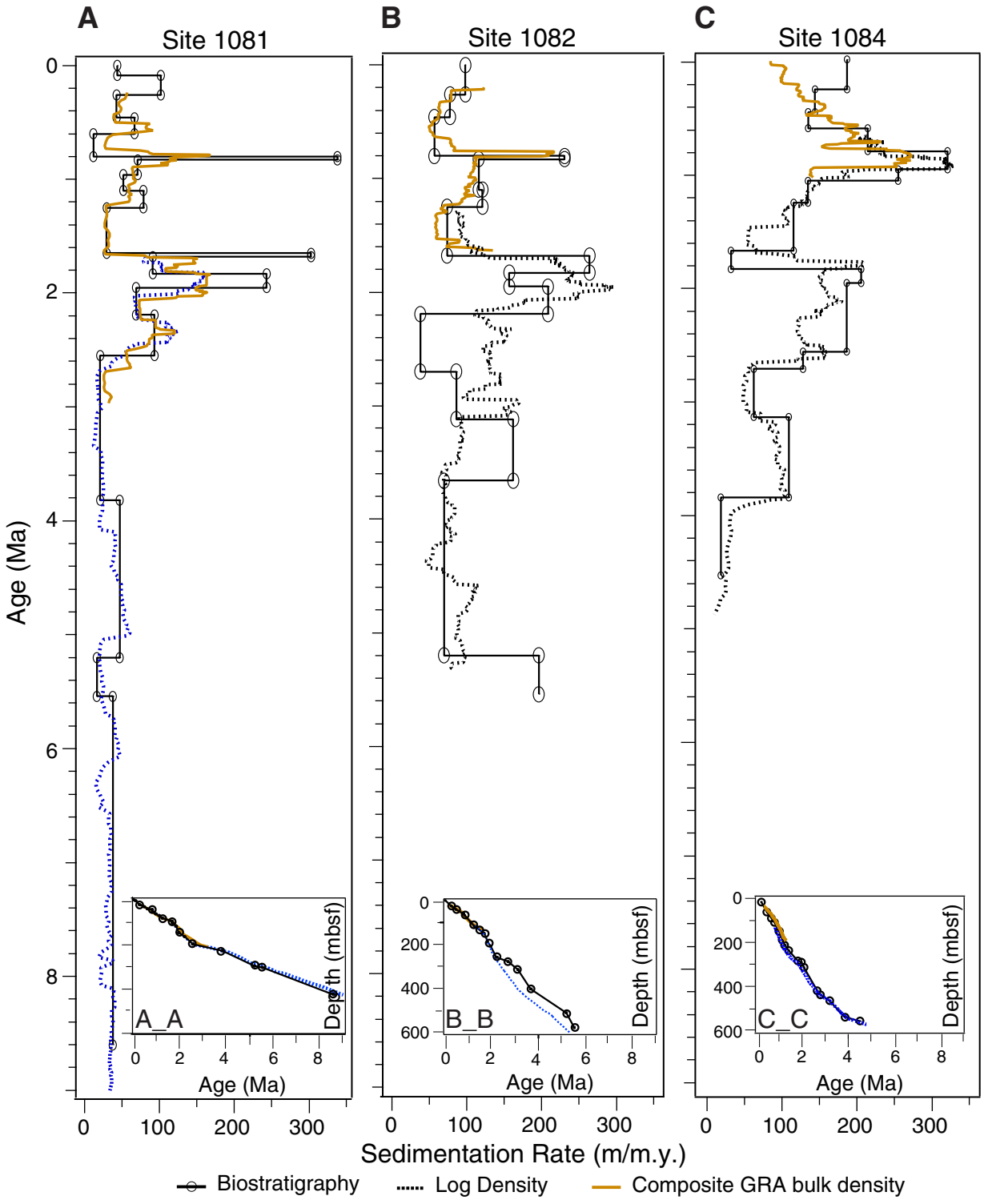

Figure F7. Spectral power in the time domain calculated from GRA bulk density records exhibit a presence of main Milankovitch cycles, namely eccentricity (10 cycles/m.y.), obliquity (24 cycles/m.y.), and precession (42 and 53 cycles/m.y.). **A.** At Site 1081 precession and obliquity are visible between 0.7 and 2.8 Ma, paralleled by eccentricity only for the past 1.5 m.y. **B, C.** Sites 1082 and 1084, where spectra were obtained for the past 1.3 m.y. only, suggest a dominance of eccentricity for this time interval. Intermittent frequencies may be explained with aliasing effects for intervals of high sedimentation rates and strong density contrasts (delta spikes), which causes individual cycles to smear out.

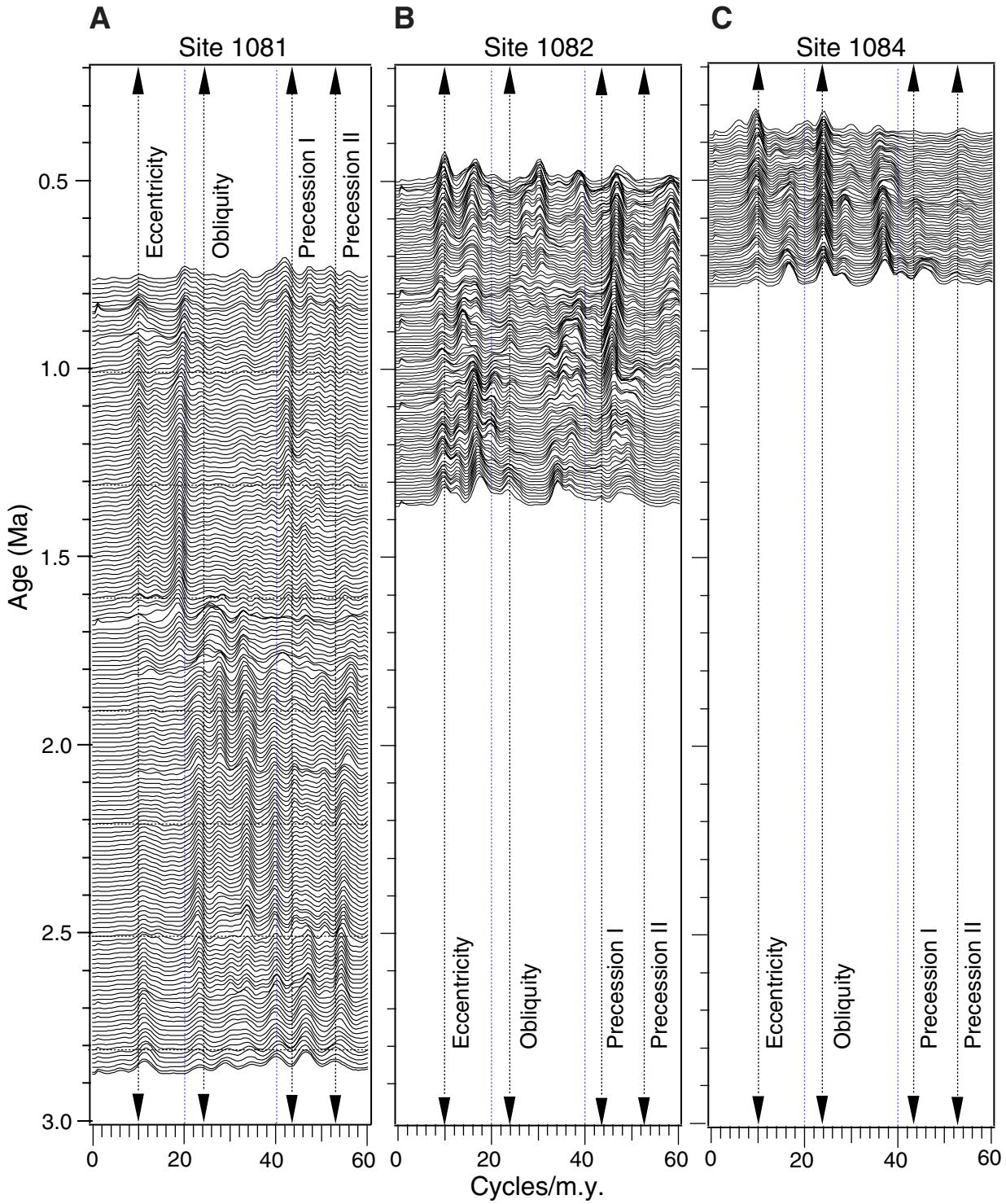

Figure F8. Spectral energy detected in log density profiles over time show cyclic patterns that match the three Milankovitch cycles at (**A**) Site 1081 between 6.0 and 4.3 Ma. Similar rhythmic patterns were observed between 3.0 and 2.2 Ma at the same site and at (**B**) Site 1082. At (**C**) Site 1084, spectral power is mainly characterized by obliquity and precession between 1.0 and 2.4 Ma, whereas eccentricity dominates thereafter. Periodicity before 6.0 Ma was only available from records at Site 1081 and shows a complex wax-and-wane pattern between eccentricity and obliquity, but no indication of precession. Intermittent frequencies are explained with noise effects induced by very strong density variations.

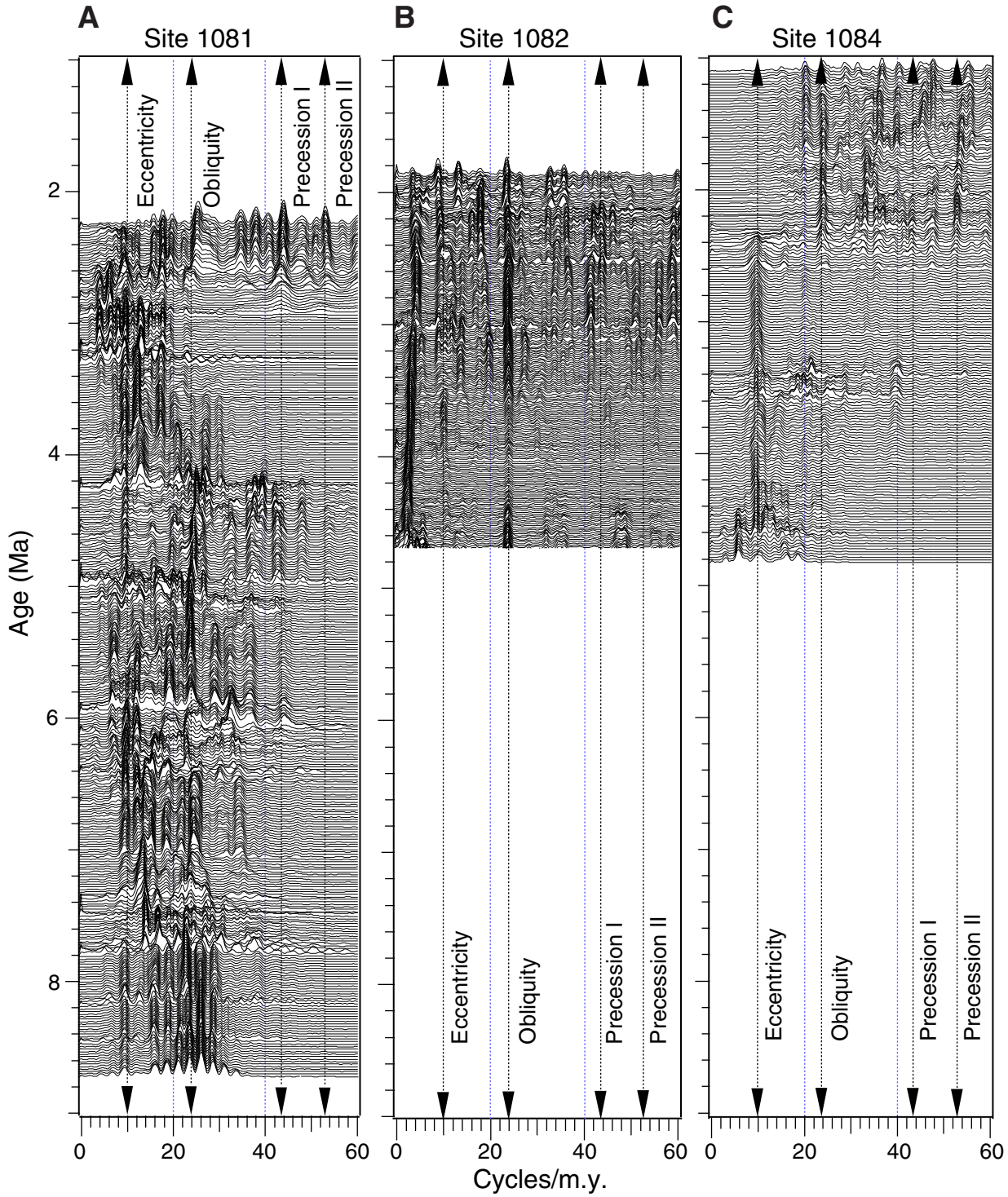

Figure F9. Synthetic sedimentation rates of three-component sediment composites (calcareous, siliceous, and clay) for a (**A**) constant, (**B**) step size, and (**C**) gradual increase of accumulation, with (**D, E, F**) corresponding synthetic density profiles.

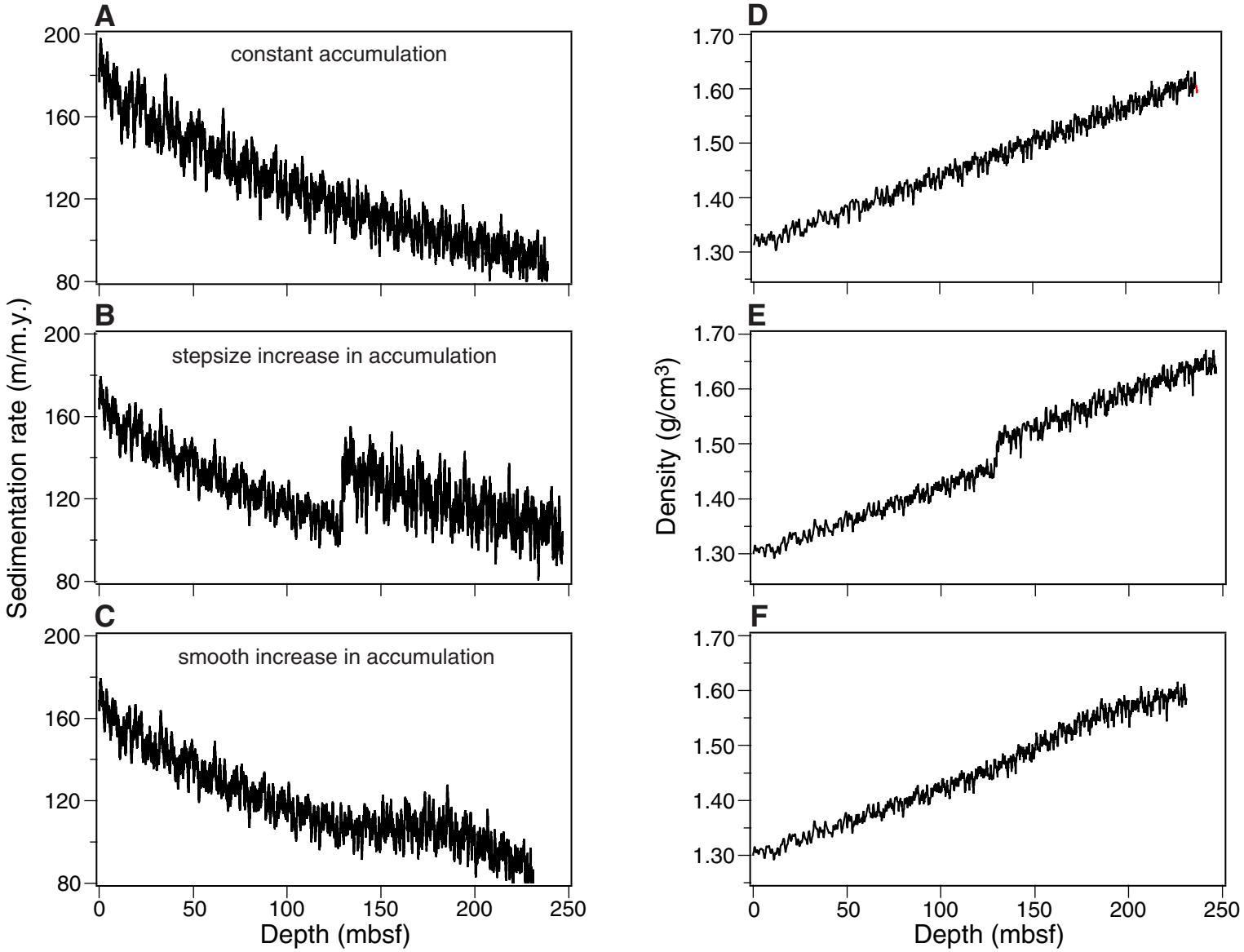

Figure F10. Various parameters that influenced results from spectral analyses include (A) smooth factor, (B) autocorrelation window length, and (C) noise introduced by delta spikes.

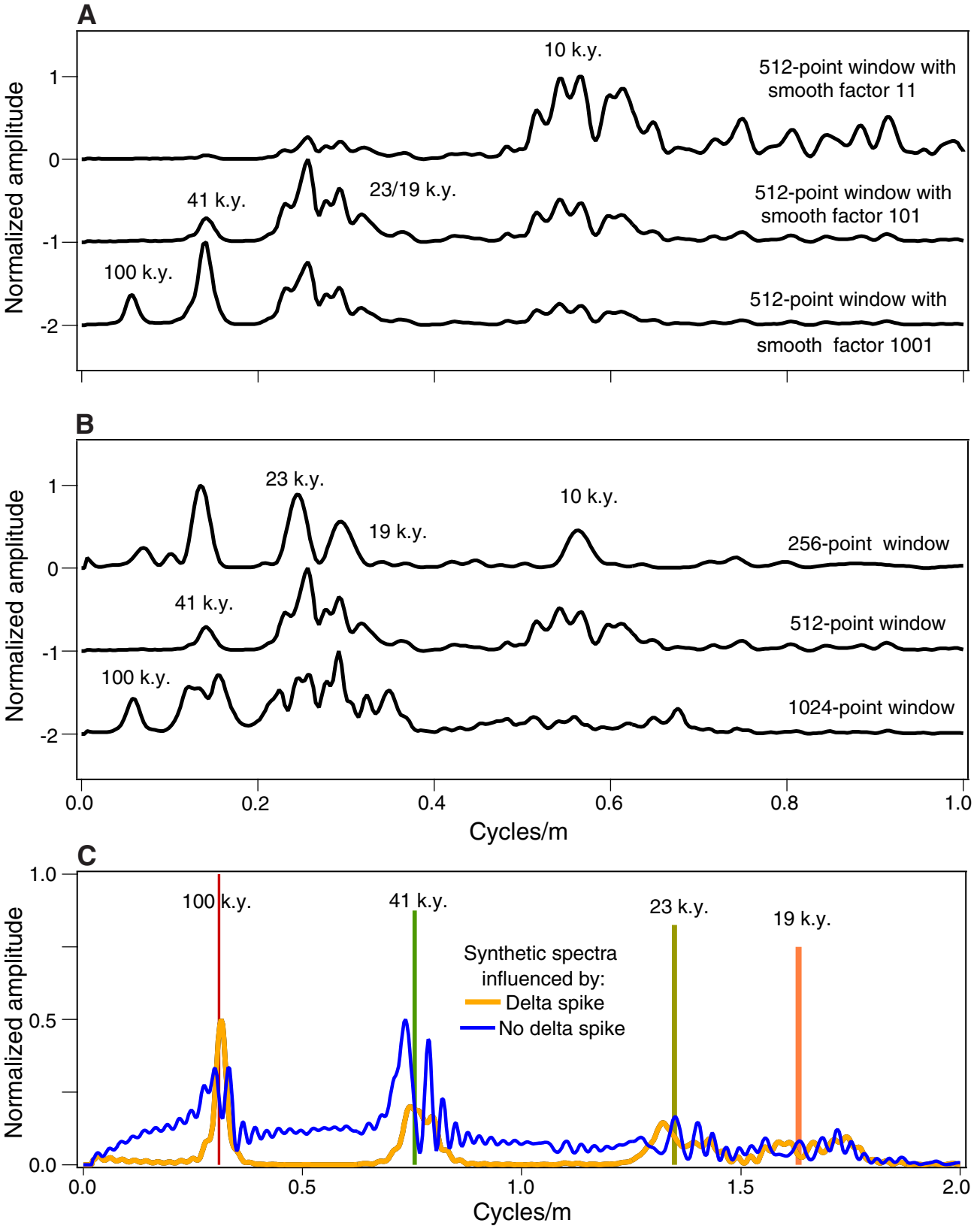

Figure F11. A. Evolutionary spectra obtained from synthetic density profiles show a gradual increase in frequency (measured in cycles per meter) with depth for constant accumulation rates (ARs). **B.** In contrast, spectra exhibit strong deflections from this pattern when ARs change rapidly. **C.** Similar but smoother effects on the profiles are observed for the gradual AR changes.

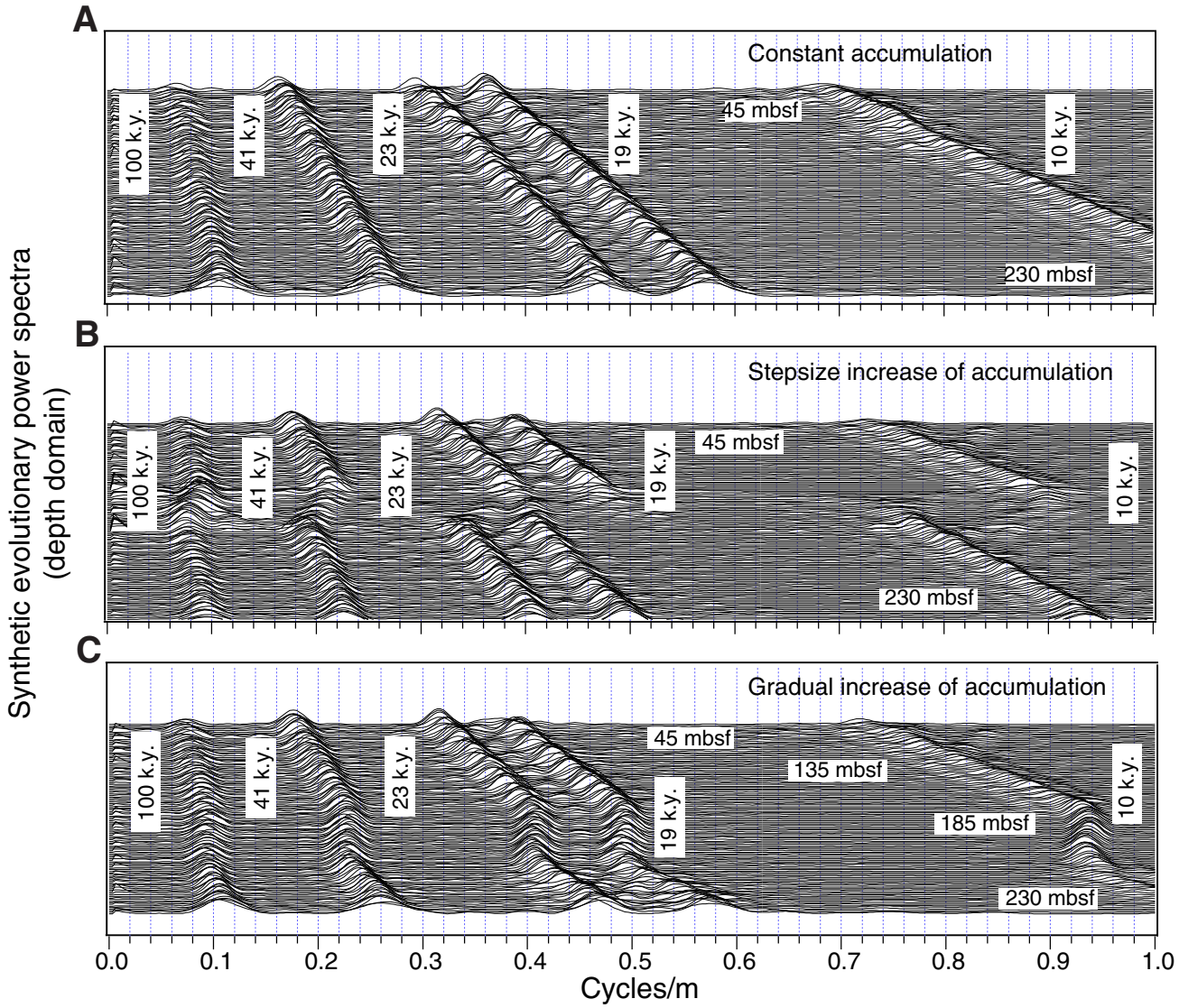

Figure F12. A. Evolutionary spectra obtained from synthetic density profiles reproduce input frequencies well over time (measured in cycles per million years) for constant accumulation rates (ARs). A slight decrease in frequency is noted for the 10-k.y. cycle, probably because of the aliasing effects. **B.** In contrast, spectra exhibit noticeable deviations from this pattern when ARs change rapidly.